DNA probes that store mechanical information reveal transient piconewton forces applied by T cells

Rong Ma[a], Anna V. Kellner[b], Victor Pui-Yan Ma[a], Hanquan Su[a], Brendan R. Deal[a], Joshua M. Brockman[b], and Khalid Salaita[a,b,1]

[a]Department of Chemistry, Emory University, Atlanta, GA 30322; and [b]Wallace H. Coulter Department of Biomedical Engineering, Georgia Institute of Technology and Emory University, Atlanta, GA 30332

Edited by Michael L. Dustin, Kennedy Institute of Rheumatology, Headington, United Kingdom, and accepted by Editorial Board Member Diane E. Griffin July 3, 2019 (received for review March 8, 2019)

The advent of molecular tension probes for real-time mapping of piconewton forces in living systems has had a major impact on mechanobiology. For example, DNA-based tension probes have revealed roles for mechanics in platelet, B cell, T cell, and fibroblast function. Nonetheless, imaging short-lived forces transmitted by low-abundance receptors remains a challenge. This is a particular problem for mechanoimmunology where ligand–receptor bindings are short lived, and a few antigens are sufficient for cell triggering. Herein, we present a mechanoselection strategy that uses locking oligonucleotides to preferentially and irreversibly bind DNA probes that are mechanically strained over probes at rest. Thus, infrequent and short-lived mechanical events are tagged. This strategy allows for integration and storage of mechanical information into a map of molecular tension history. Upon addition of unlocking oligonucleotides that drive toehold-mediated strand displacement, the probes reset to the real-time state, thereby erasing stored mechanical information. As a proof of concept, we applied this strategy to study OT-1 T cells, revealing that the T cell receptor (TCR) mechanically samples antigens carrying single amino acid mutations. Such events are not detectable using conventional tension probes. Each mutant peptide ligand displayed a different level of mechanical sampling and spatial scanning by the TCR that strongly correlated with its functional potency. Finally, we show evidence that T cells transmit pN forces through the programmed cell death receptor-1 (PD1), a major target in cancer immunotherapy. We anticipate that mechanical information storage will be broadly useful in studying the mechanobiology of the immune system.

TCR | receptor mechanics | tension sensor | PD1

Studying the interplay between mechanical forces and chemical signaling in living cells is challenging. This is due, in part, to the difficulties of detecting the piconewton (pN) forces that deform biomolecules and trigger mechanotransduction pathways. We previously developed molecular tension-based fluorescence microscopy (MTFM) to address the challenge of real-time mapping of the pN forces exerted by live cells (1). MTFM probes are anchored to a surface and composed of a spring-like element flanked by a fluorophore and quencher and presenting a biological ligand for receptor recognition (2, 3). The key design requirement for MTFM probes is to maximize fluorophore quenching when the probe is at rest and to conversely minimize quenching when the probe experiences pN force. MTFM has found a range of applications, revealing the pN forces involved in platelet activation (4) and T cell and B cell receptor triggering (5, 6), as well as cell adhesion and migration (7).

One fundamental challenge in MTFM pertains to imaging transient mechanical events. This is because MTFM probes rapidly refold (within microseconds) upon termination of the mechanical input (8). Hence, long-lived molecular forces or forces mediated by high-copy number receptors have been the focus of MTFM studies. Even single-molecule imaging of MTFM probes, which is difficult to implement in live cells, fails to capture rare mechanical events or transient mechanical events with a lifetime below that of the fluorescence acquisition time window (>100 ms) (9). One potential solution is to use the tension gauge tether (TGT) technology, which employs DNA duplex probes that are irreversibly denatured at specific thresholds of forces (10). However, the minimum detectable force threshold is ∼12 pN applied for a duration of 2 s. Additionally, rupture of the TGT terminates mechanical signaling and modulates the biological response. Hence, the TGT approach is not appropriate for detecting weak or short-lived mechanical events (10).

Thus, there is a significant need to develop new probes to detect infrequent or short-lived mechanical events actively generated by cells. Such rare mechanical events are especially important to mechanoimmunology. For example, single-molecule mechanical stimulation through the T cell receptor (TCR) peptide-major histocompatibility complex (pMHC) bond is sufficient to trigger T cells (11). Moreover, single-molecule force spectroscopy experiments show that the TCR–pMHC bond lifetime ranges from tens of milliseconds to 1 s, as a function of the applied force (1 to 20 pN) and the identity of the TCR–antigen pair (11–14). Therefore, developing molecular probes that can visualize rare and transient pN forces will provide deeper insights into mechanoimmunology.

Herein, we demonstrate the concept of dynamic mechanical information storage to record and erase molecular force signals (Fig. 1*A*). To achieve this goal, we employ the most sensitive class of MTFM probes, stem-loop DNA hairpins that function as a reversible digital switch (real-time closed; Fig. 1*A*) (5, 7). DNA

Significance

To defend against cancer and viral infections, the T cell receptor (TCR) must recognize antigens on the surface of target cells. TCR antigen recognition involves the transmission of forces which are often weak, infrequent, and short lived, and hence difficult to study. We solve this challenge by developing molecular probes that store mechanical information. This approach reveals the TCR forces when encountering different antigens, and this mechanical sampling is correlated with antigen potency. Since coreceptors are heavily involved in tuning immune function, we investigate the programmed cell death receptor 1 (PD1) and show that T cells transmit forces to this coinhibitory receptor, thus suggesting that mechanics may play a role in this important checkpoint pathway.

Author contributions: R.M. and K.S. designed research; R.M. performed experiments and analyzed data; A.V.K. provided mouse spleens and purified T cells; V.P.-Y.M. provided ICAM-1; H.S. performed atomic force microscopy; B.R.D. contributed to kinetic measurements; J.M.B. contributed to data analysis; and R.M. and K.S. wrote the paper, with all authors providing input.

The authors declare no conflict of interest.

This article is a PNAS Direct Submission. M.L.D. is a guest editor invited by the Editorial Board.

[1]To whom correspondence may be addressed. Email: k.salaita@emory.edu.

This article contains supporting information online at www.pnas.org/lookup/suppl/doi:10.1073/pnas.1904034116/-/DCSupplemental.

MTFM probes are highly modular, and the equilibrium force that leads to a 50% probability of hairpin unfolding (real-time open; Fig. 1*A*), $F_{1/2}$, can be tuned by adjusting the GC content and length of the stem-loop structure (7, 15, 16). DNA MTFM probes unfold and rapidly refold in response to forces applied by cell receptors. In our approach, storage of mechanical events is mediated by a locking oligonucleotide that selectively hybridizes to mechanically unfolded hairpins and prevents refolding (Fig. 1*B*). Therefore, mechanical unfolding of probes is irreversible upon addition of the locking strand (locked, Fig. 1*A*). The locking strand can be modified with a fluorophore, Atto647N (*SI Appendix*, Fig. S1), to report the accumulation of mechanical events that equal or exceed $F_{1/2}$. This accumulated mechanical signal can subsequently be erased by an unlocking strand that triggers a toehold-mediated strand displacement reaction (Fig. 1*A*).

Using this mechanical information storage strategy, we demonstrate the ability to perform multiple cycles of storing and erasing TCR forces, as well as mapping tension in static and migratory primary $CD8^+$ T cells. This method reveals the mechanical sampling dynamics of TCRs challenged with the antigenic pMHC, along with near-cognate pMHC ligands displaying single amino acid mutations. The results demonstrate that the TCR mechanically samples antigenic pMHCs with forces >4.7 pN, and the frequency as well as area coverage of mechanical sampling is sensitive to single amino acid mutations. Finally, the locking MTFM probes show that the programmed cell death receptor 1 (PD1), an immune checkpoint inhibitor, transmits pN forces to its ligand in primary T cells. This report demonstrates the pN force transmission through the PD1–PDL2 complex, which underscores the power of mechanical information storage in capturing fleeting mechanical events generated by low abundance receptors.

Results and Discussion

To achieve mechanical information storage, we first screened a small library of oligonucleotides to identify appropriate candidates for mechanically selective hybridization. Ideally, the locking oligonucleotide must rapidly bind to the unfolded hairpin and also display thermodynamic stability such that it remains bound to the probe for the duration of the experiment. Since the binding target is a stem-loop hairpin, these 2 properties are at odds as the most thermodynamically stable locking strand is a full complement, which will also form a hairpin itself, thus hindering the rate of locking. Conversely, shorter locking strands that lack the full stem enhance the rate of locking but reduce thermodynamic stability. Based on these criteria, we designed 5 different locking oligonucleotides that ranged in length from 25mer to 13mer to screen (*SI Appendix*, Table S1). We prepared gold nanoparticle MTFM tension probe surfaces as described previously (*SI Appendix*, Fig. S2) (5). Atomic force microscopy and fluorescence microscopy (*SI Appendix*, Fig. S3) showed that the tension probe substrates were uniform and displayed an average of 1,000 ± 89 gold nanoparticles per μm^2, with ~4.4 DNA tension probes per particle (5). Based on this screen, we used the 17mer as the locking strand due to its favorable binding (*SI Appendix*, Fig. S4). To estimate mechanoselectivity, we compared the differential binding of locking strand to MTFM probe at rest to that of an unstructured sequence (mimicking the unfolded probe) and found 2 orders of magnitude difference (*SI Appendix*, *Supplementary Note* and Fig. S5). For unlocking experiments, we engineered an 8-nt toehold with 50% GC content at the 3′ end of the locking strand. The addition of unlocking strand triggered a rapid toehold-mediated strand displacement reaction that released locking strands from the DNA probes, resetting the probes to the closed state (*SI Appendix*, Fig. S6 *A* and *B*).

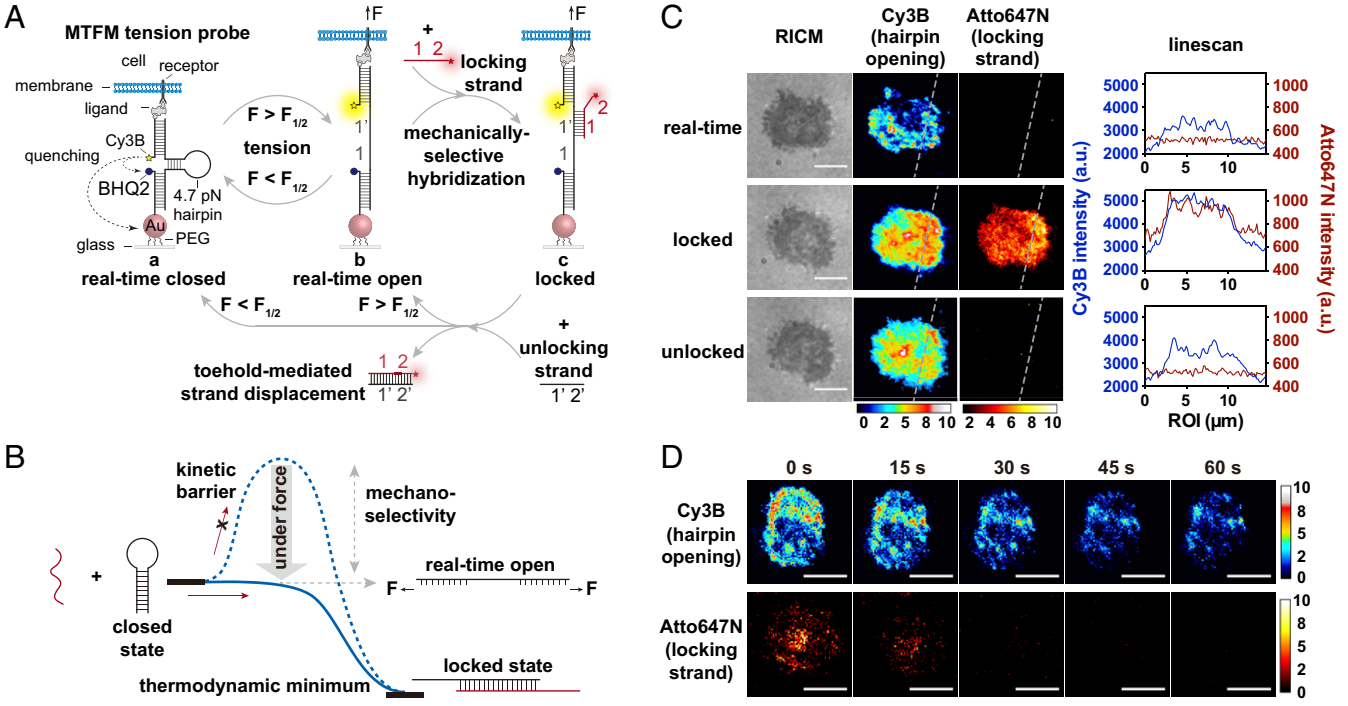

Fig. 1. (*A*) Schematic depicting the concept of mechanical information storage. (*B*) Idealized energy diagram showing how mechanical forces dampen the kinetic barrier to locking strand binding, thus affording mechanoselectivity. (*C*) RICM, Cy3B, and Atto647N TIRF images of a single OT-1 cell before and after adding the locking strand and after unlocking (toehold mediated displacement). The dashed line in the fluorescence images corresponds to the raw intensity linescan profiles shown to the right. (Scale bar, 5 μm.) (*D*) Representative cells showing the kinetics of toehold-mediated unlocking, which was visualized by the loss of signal in both the Cy3B and Atto647N channels from 2 different experiments. Images in the upper row were acquired with unlabeled locking probe, and the images in the lower row were acquired with Atto647N labeled locking probe. (Scale bar, 5 μm.) The colored bars display the contrasts used to display each set of fluorescence images.

To test the locking/unlocking concept in live cells, naïve OT-1 T cells were allowed to adhere and spread on MTFM probe surfaces presenting anti-CD3ε antibodies. Cells generated tension signal as the TCR engaged the antibody and transmitted forces to the probes (real time; Fig. 1*C*). Subsequently, the Atto647N-tagged locking strand was added for 10 min and washed, and the same T cells were imaged, confirming binding (locked; Fig. 1*C*). Importantly, the Cy3B hairpin signal increased after the locking strand was introduced (linescan; Fig. 1*C*), indicating that the locking strand led to the accumulation of opened hairpins. We found significant colocalization between the Cy3B (hairpin opening) and the Atto647N (locking strand) signals, as evident from line scan analysis and the Pearson's correlation coefficient of 0.72 ± 0.096 (n = 20 cells). Since the excess locking strand was rinsed away before reimaging, we anticipate that some mechanical hairpin unfolding events will not be accompanied by locking strand hybridization. We next tested erasing the stored cellular mechanical information. This process was triggered by adding 200 nM unlocking strand to the sample for 2–3 min and confirmed by imaging the same group of T cells (unlocked; Fig. 1*C*). The unlocking process was rapid and reached completion within 60 s (Fig. 1*D* and *SI Appendix*, Fig. S6*C*; n = 31 cells). Control experiments using tension probes with a scrambled stem-loop confirmed the specificity of locking real-time tension (*SI Appendix*, Fig. S7 *A–C*). Time lapse videos confirmed the unlocking of stored information was due to toehold-mediated strand displacement (Movie S1) rather than photobleaching (Movie S2) and was sequence-specific (*SI Appendix*, Fig. S7 *D–F* and Movies S3 and S4). Control experiments using latrunculin B (5 μM, 15 min), a cytoskeletal inhibitor, confirmed that the locked tension was maintained even when receptor forces were minimized (*SI Appendix*, Fig. S8).

One advantage of this strategy is the ability to arbitrarily toggle between the locked and unlocked states of the probe, thus selecting different time windows for integrating the force signal. Accordingly, we performed multiple rounds of mechanical information storage and erasing. TCR–anti-CD3ε forces were first imaged (real-time tension; Fig. 2*A*), and 200 nM locking strand was subsequently added to accumulate tension signal for 10 min. Excess locking strand was then washed away, and stored tension images were acquired (first cycle locked; Fig. 2*A*). The stored tension signal was then erased with 100 nM unlocking strand for 3 min (first cycle unlocked; Fig. 2*A*). This procedure was repeated for 2 additional cycles, and the hairpin opening and locking strand signal for the same naïve OT-1 cell was imaged. To quantify how locking and unlocking modulated the Cy3B tension signal, we repeated the same experiment using an unlabeled locking strand that eliminates potential bleedthrough and thus reduces the number of washes required for these measurements. Statistically significant changes were observed in integrated Cy3B intensity upon addition of locking and unlocking strand (Fig. 2*B*; n = 27 cells), corresponding to the accumulation of tension or erasing of the stored tension. The increasing levels of locked tension signal at later wash cycles may reflect the mechanosensitive nature of the TCR, which experiences shear forces during addition and washing of the oligonucleotide probes. Both inadvertent washing-induced activation of T cells and also T cell fatigue may be minimized in future studies by using microfluidics.

We next investigated the potential of mechanical information storage to map TCR forces produced by a migratory T cell (Fig.

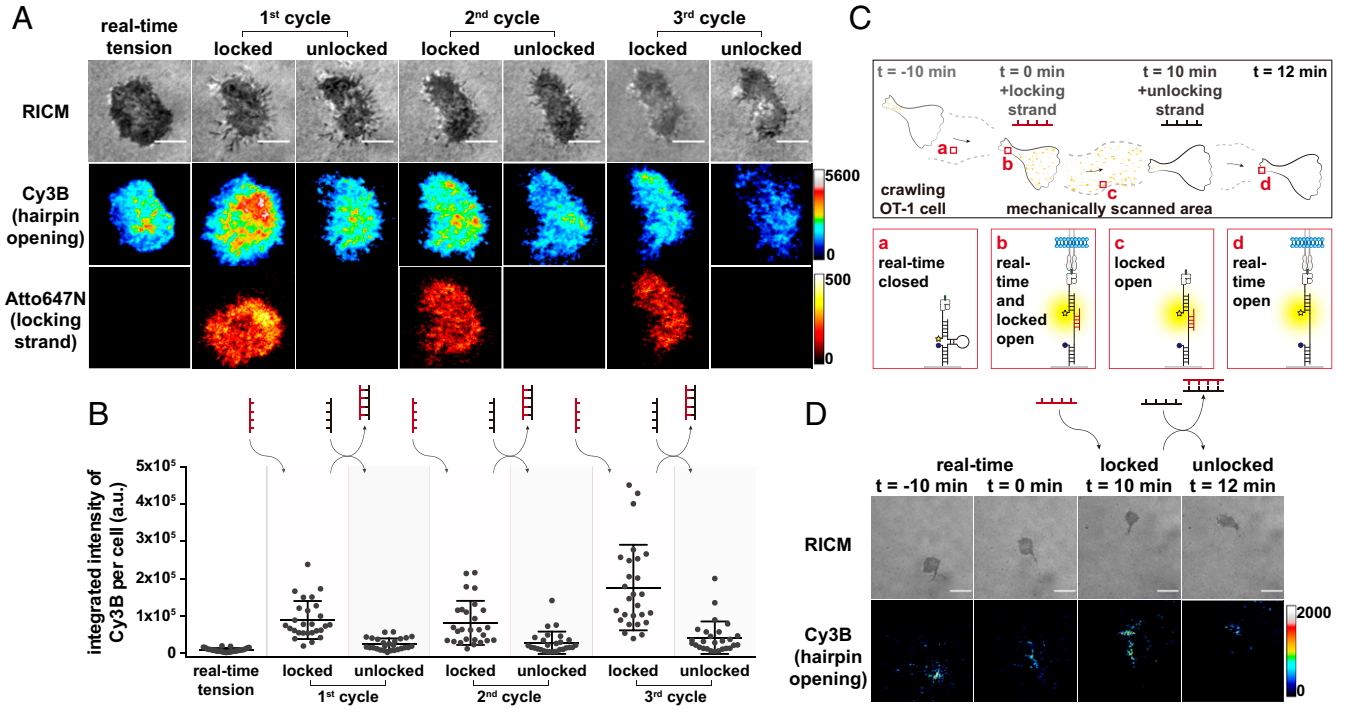

Fig. 2. (*A*) Representative RICM, Cy3B (hairpin opening), and Atto647N (locking strand) images of a single OT-1 CD8$^+$ T cell that underwent 3 rounds of mechanical information storage and erasing. (Scale bar, 5 μm.) Locking was driven with a 200 nM solution of oligo for a duration of 10 min, while unlocking was triggered using 100 nM unlocking probe for a duration of 3 min. The Atto647N signal drops to background levels upon addition of the unlocking strand. The colored bars display the contrasts used to display each set of fluorescence images. (*B*) Plot displaying the Cy3B (hairpin opening) integrated intensity per cell for a population of cells (n = 27 cells) that underwent 3 cycles of locking and unlocking as described in *A*, except for using an unlabeled locking strand instead of a Atto647N labeled locking strand. Error bars represent SD. There was a statistically significant shift in the integrated intensity based on Student's t tests when comparing locked to unlocked groups, $P < 0.0001$. (*C*) Schematic showing how mechanical information storage was used to map mechanical sampling/scanning of pMHC antigen during cell migration. (*D*) Representative RICM and tension images of a single T cell crawling on an ICAM-1/pMHC N4 surface. The first 2 images correspond to 2 time points acquired in the real-time state (before locking). The third image was collected after adding the locking strand for 10 min (revealing tension history), and the fourth image shows the tension signal after unlocking. (Scale bar, 10 μm.)

2*C*). To trigger the migration, we engineered surfaces presenting ICAM-1 molecules along with the antigenic N4 pMHC (peptide: SIINFEKL), which is a commonly studied OT-1 TCR antigen (17). ICAM-1 binds to lymphocyte function-associated antigen 1 (LFA-1), which is crucial in T cell activation, adhesion, and crawling (18). The copresentation of these 2 ligands triggered a highly migratory phenotype of OT-1 cells (Movie S5). The TCR tension was primarily located at the trailing edge of the cells and was highly transient, dynamically following the cellular trajectory along the substrate (real-time; Fig. 2*D* and Movie S5). Motile T cells show a distinct TCR force map compared with static cells exclusively stimulated with N4 pMHC; the latter formed a ring-like tension pattern that evolved to distribute across the cell–substrate contact area (Fig. 3*A*) (5). Upon addition of the locking strand, the TCR tension signal was enhanced and also extended across the T cell track, revealing the spatial distribution of pMHC ligands scanned with $F > 4.7$ pN over 10 min (locked; Fig. 2*D*). Interestingly, these images show that the T cell mechanically scanned a significant fraction of antigen (81 ± 28% over its initial contact area, $n = 10$ cells) within a 10-min migration time window. Thus, the dynamic T cell synapse (kinapse) represents a zone of TCR mechanosensing (19–21). Upon addition of the unlocking strand, probes reset back to the real-time state and exclusively showed tension at the trailing cell edge (unlocked state; Fig. 2*D*). Taken together, these experiments show the utility of the locking/unlocking strategy to visualize the molecular forces associated with static and migratory T cells across different time scales.

Given that mechanolocking enhances TCR–pMHC tension signal by accumulating pulling events that are >4.7 pN, we next aimed to determine the degree of enhancement and its accumulation dynamics. OT-1 T cells were allowed to engage real-time tension probes and then incubated with unlabeled locking strand (200 nM). The unlabeled locking strand was beneficial here because it eliminated bleedthrough from Atto647N and reduced rinsing steps. Fig. 3*A* shows a time course for TCR-N4 pMHC tension signal accumulation for 3 cells upon addition of the locking strand. Interestingly, the tension signal was concentrated at the central and peripheral region of the cell–substrate interface and accumulated over time after lock strand addition (*SI Appendix*, Fig. S9). Analysis of kinetics for $n = 16$ cells showed that the signal approached saturation by $t = 10$ min (Fig. 3*B*). Notably, the enhancement of the integrated N4 tension signal per cell was ∼189-fold in this experiment. Tension occupancy, which is the fraction of the cell contact area showing tension signal, reached 91% in 10 min. The tension occupancy is an indication of the area that is mechanically scanned by the TCR with F > 4.7 pN in search for antigen. The kinetics of the tension occupancy increase is in agreement with a recent report showing that T cell microvilli search for cognate antigen at a consistent coverage (22).

We next sought to investigate how T cells differentially mechanically sample their cognate and near-cognate ligands over

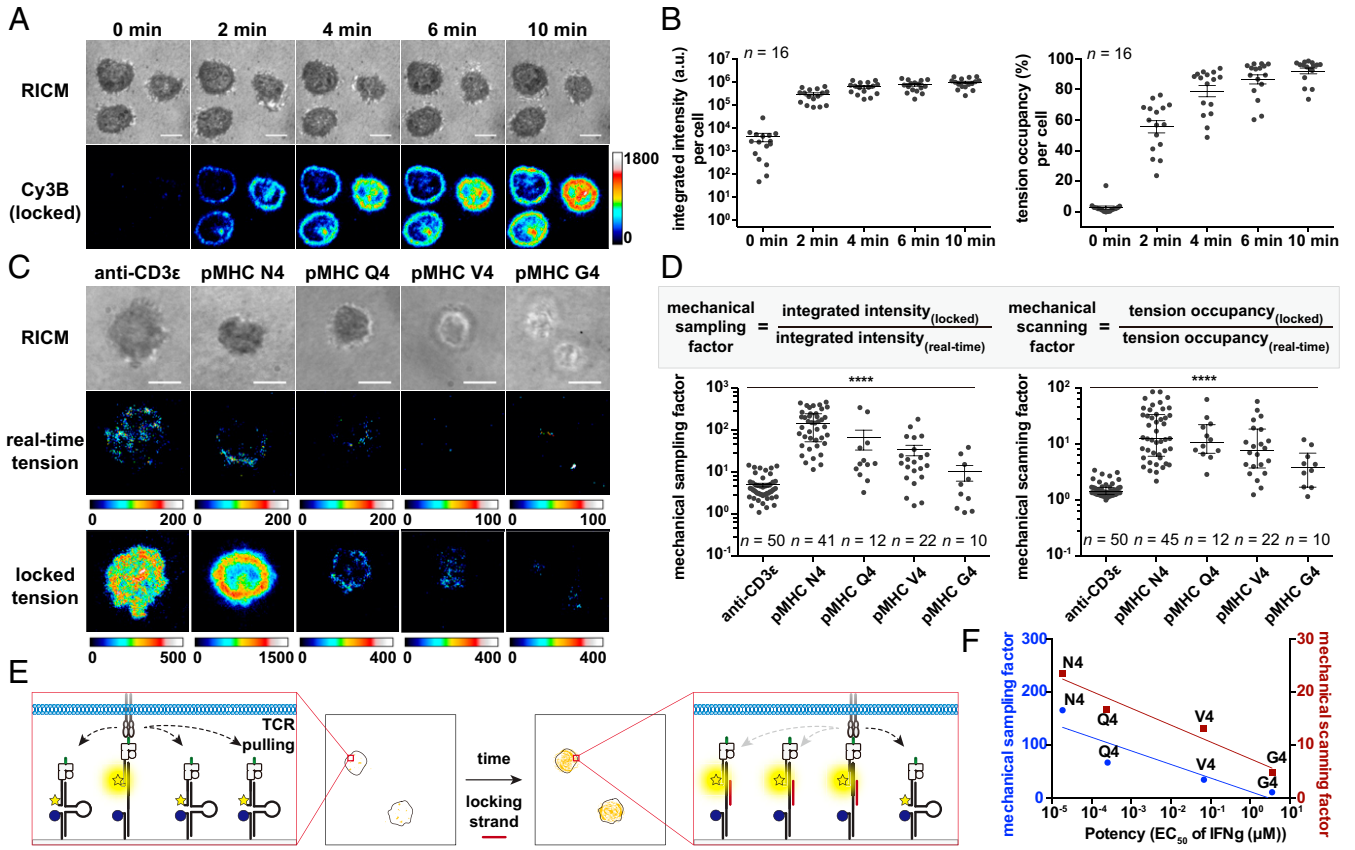

Fig. 3. (*A*) Time lapse showing RICM and Cy3B tension signal for 3 representative cells after adding locking strand to probes presenting N4 ligand. (Scale bar, 5 μm.) (*B*) Plots of integrated tension signal and tension occupancy of individual cells as a function of time ($n = 16$ cells from the same animal). Error bars represent the SEM. (*C*) Representative images of single cells that were imaged using probes in the real-time and locked state when presented with anti-CD3ε, pMHC N4, Q4, V4, and G4. Note the colored bars at the bottom of each image indicate the range of display values and differ for each group depending on the intensity of the signal. (Scale bar, 5 μm.) (*D*) Definition and plots showing sampling and scanning factor for different ligands. Error bars represent the SEM. Statistical significance was analyzed with a 1-way ANOVA (****$P < 0.0001$). The number of analyzed cells in each group is indicated in the plots. (*E*) Schematic showing the concept of mechanical sampling and scanning. (*F*) Correlation between the mechanical sampling and scanning factor and the potency of the ligand. EC_{50} values were obtained from literature (24).

time. The TCR–pMHC interaction is highly specific, allowing T cells to discriminate between single amino acid mutants of the cognate pMHC despite their similar μM-range 3D affinity (23). Single-molecule force spectroscopy measurements suggest that the stability of the TCR–pMHC complex at differing levels of mechanical strain provides a mechanism to enhance antigen discrimination (12). We tested a panel of well-characterized altered peptide ligands, as well as anti-CD3ε, against OT-1 cells. Fig. 3*C* shows representative TCR tension maps of naïve OT-1 cells challenged with the cognate N4 pMHC and single amino acid mutants of the fourth position of SII**X**FEKL, where X = Q, V, and G. In the real-time state, cells produced the greatest tension signal with anti-CD3ε, followed by N4, with the mutant pMHC antigens producing weak or nondetectable tension signal. This result is consistent with our prior work with V4 (5) and also with the reported bond lifetimes for mutant ligands (11). For example, independent of CD8, TCR-pMHC N4 binding displays catch-bond behavior, with an average bond lifetime of 100 ms at 0 pN and 800 ms at 10 pN. However, the TCR exhibits slip-bond behavior with the mutant pMHC G4 (SII**G**FEKL), displaying an average bond lifetime of 300 ms at 0 pN and <100 ms at 10 pN (11, 23). Such short-lived mechanical events are difficult to visualize with conventional MTFM probes. Upon addition of the locking strand, the integrated tension signal was significantly enhanced in all of the tested antigens. Although mechanical events mediated between TCRs and weak antigens are transient and previously undetectable, the addition of the locking strand amplified the tension signal and rendered it detectable (locked tension; Fig. 3*C*). The less potent pMHC Q4 produced a ring pattern that could be observed after locking, although it was much less pronounced compared with the N4 antigen. With pMHC V4 and G4, tension did not show the typical ring pattern and was more disorganized. The mutant antigens showed significantly weaker integrated tension and tension occupancy, which can be attributed, in part, to TCR–pMHC bond failure as well as the lack of T cell triggering.

We noticed that the signal accumulation levels differed when cells were presented with antibody, cognate pMHC, and altered peptide ligands. To quantify these differences on a per cell basis, we defined 2 parameters: the mechanical sampling factor, which is the fold enhancement in integrated tension signal, and the mechanical scanning factor, which reflects the fold increase in tension occupancy (Fig. 3*D*). These factors reflect the frequency of TCR binding to antigens, applying F > 4.7 pN, dissociating, and then sampling new ligands (Fig. 3*E*). Interestingly, the integrated tension signal and the tension occupancy varied significantly for different antigens (*SI Appendix*, Fig. S10). Plots in Fig. 3*D* show the mechanical sampling and mechanical scanning factors for different TCR ligands averaged from $n > 10$ cells per group. Surprisingly, the average mechanical sampling factor was only 5 ± 0.5 (mean ± SEM) for anti-CD3ε, whereas for N4 it was 165 ± 21, followed by 66 ± 32, 33 ± 9, and 10 ± 4 for the Q4, V4, and G4 antigens, respectively (Fig. 3*D* and *SI Appendix*, Fig. S10*A*). Although the real-time tension with anti-CD3ε was the greatest among all tested ligands (Fig. 3*C*), it failed to accumulate as fast as N4, implying less frequent mechanical sampling by the TCRs, which is likely partially due to the slow k_{off} of the antibody. The difference in 2D kinetics of TCR–ligand interactions is likely an important contributor to the significant difference in mechanical sampling factor across the panel of altered peptide ligands. For example, independent of CD8 engagement, the TCR–pMHC N4 interaction has an effective 2D on-rate $A_c k_{on} = 1.7 \times 10^{-3}$ μm^4 s^{-1} at 25 °C (23). This rapid on-rate enables T cells to search for and sample antigens at high speed and quickly accumulate sufficient antigen stimulation for further signaling. In contrast, for less potent pMHC G4, $A_c k_{on} = 4.7 \times 10^{-5}$ μm^4 s^{-1} (23), which contributes to a smaller mechanical sampling factor. There has been long standing speculation that the rapid kinetics of TCR–antigen binding provides an advantage in terms of maximizing sampling of antigen. Our results confirm this notion through the mechanical sampling factor for N4.

The mechanical scanning factor, which is a measure of the increase in tension occupancy and is related to cytoskeleton coordination of TCRs, showed similar trends. Before locking, the tension occupancy for the anti-CD3ε and N4 ligands was 60.8 ± 2.1% (mean ± SEM) and 8.3 ± 1.1%, respectively (real time; Fig. 3*C* and *SI Appendix*, Fig. S10*B*). After locking, the tension occupancy increased to 88.7 ± 1.2% and 90.6 ± 1.4% for anti-CD3ε and N4, respectively (locked; Fig. 3*C* and *SI Appendix*, Fig. S10*B*), leading to a scanning factor of 1.6 ± 0.1 (mean ± SEM) for anti-CD3ε and 23.6 ± 3.3 for N4. Within 10 min of contacting the surface, cells leveraged the short-lived TCR–pMHC N4 bond to mechanically scan almost the entire contact area, significantly faster than the cells on anti-CD3ε substrate, although both ligands can activate T cells effectively. Moreover, the locked tension signal showed a ring pattern with puncta at its center (pMHC N4; Fig. 3*C*), demonstrating that the most frequent pulling events were arranged and focused at the edge and the center of the cells. This pattern resembles the architecture of the immunological synapse. With the altered peptide ligands, the decreased scanning factor (Fig. 3*D*), together with the reduced contact area (pMHC Q4, V4, G4; Fig. 3*C*), suggest weaker cytoskeleton engagement, which might be an outcome of reduced cell triggering. These direct measurements of TCR mechanical sampling and scanning agree well with previous single-molecule force spectroscopy measurements, where forces were applied externally to determine 2D kinetics and affinity (23). We also found that the mechanical sampling and scanning factors were both highly correlated to the potency of these antigens (as measured using published cytokine production assays) (24, 25), further underscoring the potential of these mechanical parameters as readouts of T cell activation (Fig. 3*F*).

Although TCR–pMHC affinities are weak (K_d~μM), T cells tend to express high copy numbers of the TCR. The reported density of TCRs in naïve OT-1 cells is ~130 to 200 molecules per μm^2 (23). To demonstrate mapping of forces generated by low abundance receptors, we next investigated mechanotransduction of the PD1. PD1 is a coinhibitory receptor that down-regulates T cell activation when it encounters its ligands, programmed cell death ligand 1 (PDL1), and/or ligand 2 (PDL2) (26). PD1 density is low in naïve OT-1 CD8$^+$ cells, with 0.2 molecules per μm^2 (24 ± 1 copies per cell) and 6.8 molecules per μm^2 (671 ± 16 copies per cell) in antibody-stimulated activated cells (27). Hence, we activated naïve OT-1 cells using the N4 peptide for 48 h (see *SI Appendix, Materials and Methods*), and the activated cells were imaged on tension probes presenting either anti-PD1 antibody or murine PDL2. TCR–anti-CD3ε forces were also

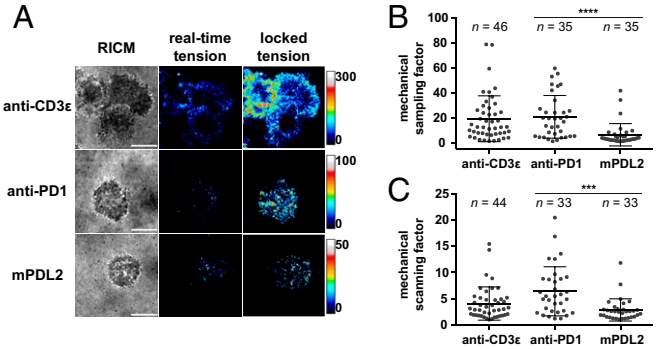

Fig. 4. (*A*) Representative RICM and tension images of activated OT-1 cells on anti-CD3ε, anti-PD1, and mPDL2-functionalized tension probes in the real-time and locked state (10 min duration). (Scale bar, 10 μm.) Colored bars indicated the display values used for each set of fluorescence images. (*B* and *C*) Plots of mechanical sampling factor and mechanical scanning factor for anti-CD3ε, anti-PD1, and mPDL2 in activated OT-1 cells. Error bars represent SD (statistical significance was analyzed with a Student's *t* test; ***$P < 0.001$; ****$P < 0.0001$).

quantified as a positive control. Without the locking strand, the PD1–anti-PD1 and PD1-mPDL2 tension was very weak or nondetectable (real-time; Fig. 4*A*). However, the PD1 tension signal was enhanced upon addition of the locking strand (1 μM, introduced 30 min after cell plating) (locked; Fig. 4*A*). In contrast to TCR forces, PD1–mPDL2 tension was less abundant and more punctate and did not display a typical ring-pattern characteristic for TCR ligands. The integrated tension intensity and tension occupancy were quantified before and after incubation with the locking strand (*SI Appendix*, Fig. S11). Both parameters were weaker for the mPDL2 ligand compared with the PD1 antibody, likely reflective of their relative affinities (28). Even upon addition of the locking strand, there was modest signal enhancement compared with that of the TCR antigens. Employing similar parameters defined in Fig. 3*D*, we found that the mechanical sampling factor was 6.4 ± 1.5 for mPDL2 and 20.8 ± 2.9 for anti-PD1 (Fig. 4*B*). The mechanical scanning factor was 2.9 ± 0.4 for mPDL2 and 6.4 ± 0.8 for anti-PD1 (Fig. 4*C*). These values imply that PD1 forces were less dynamic when T cells were stimulated with mPDL2 compared with anti-PD1. Given that PD1–PDL2 binding mediates dampening of T cell activity and adhesion (29), it is plausible that this difference reflects differential T cell activation upon stimulation with PDL2 versus anti-PD1. Taken together, the mechanical information storage approach clearly shows that PD1 transmits F > 4.7 pN to its ligand upon surface engagement. Future studies are needed to determine whether and how mechanical forces modulate PD1 signaling.

Conclusion

This work implements a strategy that can switch between mapping the real-time receptor force and accumulated force history and overcomes the shortcomings in mapping weak and transient mechanical events that are characteristic of immune receptor interactions. By employing multiple tension locking and unlocking cycles, we demonstrate the utility of this technique for studying both static and migratory cell mechanics. This method was further applied to visualize and analyze TCR forces upon engagement to cognate antigen and altered peptide ligands. With this technique, we were able to define mechanical sampling–scanning factors that correlated with ligand potency. Moreover, this strategy revealed PD1 receptor mechanics, featuring a punctate pattern with a less dynamic sampling profile than the TCR. Mechanical locking represents a significant improvement in sensitivity for molecular tension probes, and therefore, it may become the standard in the field when studying mechanoimmunology. We recognize 2 potential limitations of mechanical information storage. First, the signal enhancement comes at a cost of losing temporal information; thus, this method cannot capture the oscillatory dynamics of T cell forces (30, 31). Second, the addition of locking strand slightly tilts the energy landscape of hairpins toward the open state, which will reduce the effective $F_{1/2}$ in a concentration-dependent manner. Nonetheless, this work demonstrates a powerful strategy to investigate weak, transient, and less abundant mechanical events, which is expected to be widely useful for studying the mechanobiology of immune cells.

Materials and Methods

Surface Preparation. Activated glass coverslips were functionalized with a dense layer of gold nanoparticles. Thiolated DNA tension probes were then anchored to the gold particles presenting appropriate ligands (pMHCs, anti-CD3ε, anti-PD1, or mPDL2).

Cells. All experiments were performed with purified $CD8^+$ primary OT-1 cells that were either naïve (for TCR measurements) or activated (for PD1 measurements).

Imaging. Microscopy was performed using a Nikon Eclipse Ti system equipped with Evolve EMCCD (Photometrics), an Intensilight epifluorescence source (Nikon), a CFI Apo 100× NA 1.49 objective (Nikon), and a TIRF launcher with 3 laser lines: 488 nm (10 mW), 561 nm (50 mW), and 638 nm (20 mW).

ACKNOWLEDGMENTS. The work was supported by NIH Grants R01GM131099, NIH R01GM124472, and NSF CAREER 1350829. V.P.-Y.M. was supported by National Cancer Institute (NCI) Fellowship F99CA223074. J.M.B. was supported by NCI Fellowship F99CA234959 and by NSF Graduate Research Fellowship Program 1444932. We thank Dr. Cheng Zhu and Dr. Kaitao Li (Georgia Institute of Technology) for providing mutant pMHCs and mPDL2, as well as discussions. We thank Dr. Brian Evavold (University of Utah) for helpful discussions. We thank the NIH Tetramer Facility for pMHC ligands. This study was supported, in part, by the Emory Comprehensive Glycomics Core.

1. D. R. Stabley, C. Jurchenko, S. S. Marshall, K. S. Salaita, Visualizing mechanical tension across membrane receptors with a fluorescent sensor. *Nat. Methods* **9**, 64–67 (2011).
2. Y. Liu, K. Galior, V. P. Ma, K. Salaita, Molecular tension probes for imaging forces at the cell surface. *Acc. Chem. Res.* **50**, 2915–2924 (2017).
3. V. P.-Y. Ma, K. Salaita. DNA nanotechnology as an emerging tool to study mechanotransduction in living systems. *Small* 15, 10.1002/smll.201900961 (2019).
4. Y. Zhang *et al.*, Platelet integrins exhibit anisotropic mechanosensing and harness piconewton forces to mediate platelet aggregation. *Proc. Natl. Acad. Sci. U.S.A.* **115**, 325–330 (2018).
5. Y. Liu *et al.*, DNA-based nanoparticle tension sensors reveal that T-cell receptors transmit defined pN forces to their antigens for enhanced fidelity. *Proc. Natl. Acad. Sci. U.S.A.* **113**, 5610–5615 (2016).
6. K. M. Spillane, P. Tolar, B cell antigen extraction is regulated by physical properties of antigen-presenting cells. *J. Cell Biol.* **216**, 217–230 (2017).
7. Y. Zhang, C. Ge, C. Zhu, K. Salaita, DNA-based digital tension probes reveal integrin forces during early cell adhesion. *Nat. Commun.* **5**, 5167 (2014).
8. Y. Yin, X. S. Zhao, Kinetics and dynamics of DNA hybridization. *Acc. Chem. Res.* **44**, 1172–1181 (2011).
9. M. F. Juette *et al.*, The bright future of single-molecule fluorescence imaging. *Curr. Opin. Chem. Biol.* **20**, 103–111 (2014).
10. X. Wang, T. Ha, Defining single molecular forces required to activate integrin and notch signaling. *Science* **340**, 991–994 (2013).
11. B. Liu, W. Chen, B. D. Evavold, C. Zhu, Accumulation of dynamic catch bonds between TCR and agonist peptide-MHC triggers T cell signaling. *Cell* **157**, 357–368 (2014).
12. J. Hong *et al.*, A TCR mechanotransduction signaling loop induces negative selection in the thymus. *Nat. Immunol.* **19**, 1379–1390 (2018).
13. D. K. Das *et al.*, Force-dependent transition in the T-cell receptor β-subunit allosterically regulates peptide discrimination and pMHC bond lifetime. *Proc. Natl. Acad. Sci. U.S.A.* **112**, 1517–1522 (2015).
14. L. V. Sibener *et al.*, Isolation of a structural mechanism for uncoupling T cell receptor signaling from peptide-MHC binding. *Cell* **174**, 672–687.e27 (2018).
15. M. T. Woodside *et al.*, Nanomechanical measurements of the sequence-dependent folding landscapes of single nucleic acid hairpins. *Proc. Natl. Acad. Sci. U.S.A.* **103**, 6190–6195 (2006).
16. B. L. Blakely *et al.*, A DNA-based molecular probe for optically reporting cellular traction forces. *Nat. Methods* **11**, 1229–1232 (2014).
17. S. R. Clarke *et al.*, Characterization of the ovalbumin-specific TCR transgenic line OT-I: MHC elements for positive and negative selection. *Immunol. Cell Biol.* **78**, 110–117 (2000).
18. B. L. Walling, M. Kim, LFA-1 in T cell migration and differentiation. *Front. Immunol.* **9**, 952 (2018).
19. V. Mayya *et al.*, Durable interactions of T cells with T cell receptor stimuli in the absence of a stable immunological synapse. *Cell Rep.* **22**, 340–349 (2018).
20. G. A. Azar, F. Lemaître, E. A. Robey, P. Bousso, Subcellular dynamics of T cell immunological synapses and kinapses in lymph nodes. *Proc. Natl. Acad. Sci. U.S.A.* **107**, 3675–3680 (2010).
21. M. L. Dustin, T-cell activation through immunological synapses and kinapses. *Immunol. Rev.* **221**, 77–89 (2008).
22. E. Cai *et al.*, Visualizing dynamic microvillar search and stabilization during ligand detection by T cells. *Science* **356**, eaal3118 (2017).
23. J. Huang *et al.*, The kinetics of two-dimensional TCR and pMHC interactions determine T-cell responsiveness. *Nature* **464**, 932–936 (2010).
24. C. Godinho-Silva *et al.*, Defining immune engagement thresholds for in vivo control of virus-driven lymphoproliferation. *PLoS Pathog.* **10**, e1004220 (2014).
25. S. G. Oberle *et al.*, A minimum epitope overlap between infections strongly narrows the emerging T cell repertoire. *Cell Rep.* **17**, 627–635 (2016).
26. A. H. Sharpe, K. E. Pauken, The diverse functions of the PD1 inhibitory pathway. *Nat. Rev. Immunol.* **18**, 153–167 (2018).
27. E. Hui *et al.*, T cell costimulatory receptor CD28 is a primary target for PD-1-mediated inhibition. *Science* **355**, 1428–1433 (2017).
28. K. Li, X. Cheng, A. Tilevik, S. J. Davis, C. Zhu, In situ and in silico kinetic analyses of programmed cell death-1 (PD-1) receptor, programmed cell death ligands, and B7-1 protein interaction network. *J. Biol. Chem.* **292**, 6799–6809 (2017).
29. I. Azoulay-Alfaguter, M. Strazza, A. Pedoeem, A. Mor, The coreceptor programmed death 1 inhibits T-cell adhesion by regulating Rap1. *J. Allergy Clin. Immunol.* **135**, 564–567.e1 (2015).
30. C. A. Hartzell, K. I. Jankowska, J. K. Burkhardt, R. S. Lewis, Calcium influx through CRAC channels controls actin organization and dynamics at the immune synapse. *eLife* **5**, e14850 (2016).
31. T. N. Sims *et al.*, Opposing effects of PKCtheta and WASp on symmetry breaking and relocation of the immunological synapse. *Cell* **129**, 773–785 (2007).